Defence Science Journal, Vol. 62, No. 4, July 2012, pp. 252-260, DOI: 10.14429/dsj.62.1279

Effect of Trivalent Additions and Processing on Structural and Magnetic Transitions in *Ni-Mn-Ga* Ferromagnetic Shape Memory Alloys

R.P. Mathur*, R.K. Singh, S. Ray[!], P. Ghosal, and V. Chandrasekaran

Defence Metallurgical Research Laboratory, Hyderabad-500 058, India
[!]Indian Institute of Technology, Roorkee-247 667, India
**E-mail: mathur@dmrl.drdo.in*

ABSTRACT

Ferromagnetic shape memory $Ni_{50}Mn_{30}Ga_{15}Al_{5-x}B_x$ (x = 0, 1, and 4) alloys were prepared by vacuum arc melting and subsequent heat-treatment as well as by melt spinning to investigate the effect of trivalent element additions in ternary *Ni-Mn-Ga* alloys. The heat-treated alloys containing *Al* were reported to possess a modulated martensite structure, however alloy containing both *Al* and *B* showed a loss of modulated structure in martensite formed. The rapidly solidified alloys on the other hand showed the formation of a similar modulated structure without composition change in alloys containing *Al* and the alloys containing *Al* and *B*. In addition, the former showed a presence of an amorphous phase with latter showing crystalline boron rich phases. The magnetisation of the *B* containing alloys in both the processing technique was however very low, showing lower magnetic exchange interaction in such alloys.

Keywords: Ferromagnetic shape memory alloys, *Ni-Mn-Ga* alloys, martensitic transformation

1. INTRODUCTION

Ferromagnetic shape memory (FMSM) alloys are emerging as active materials for smart devices such as sensors, actuators, and transducers due to an optimal combination of work output and response time for the devices[1]. Alloys based on Heusler Ni_2MnGa compositions have shown large magnetic field induced strains of magnitude 6-10 per cent at room temperatures[2-5]. The stoichiometric Ni_2MnGa alloy has an $L2_1$ structure and undergoes a magnetic transition at 376 K and structural martensite transformation at 202 K to martensite structure. The martensite phase stability is affected by average valance electrons per atom (e/a ratio). For *Ni-Mn-Ga* alloys, e/a ratio is estimated using ten, seven, and three valance electrons for *Ni*, *Mn,* and *Ga* atom respectively[6,7]. Both *Ni* and *Mn* substitutions for *Ga* increase the e/a ratio and thereby martensite transformation temperatures[8,9]. *Mn*-rich compositions are employed for FMSM applications as they exhibit modulated martensite structure with low de-twining stresses[4,8]. The *Mn*-substitution however, lowers the Curie temperature[8]. Ternary $Ni_{50}Mn_{30}Ga_{20}$ (atom %) with e/a ratio of 7.7 shows the maximum operating temperatures possible as martensite transformation approaches Curie temperature and modulated martensite structure is unstable[10]. The addition of other tri-valent elements for *Ga* may affect the inter-atomic distances thereby stabilizing the modulated structures without changing the e/a ratio or affecting the transformation temperatures.

The martensite transformation temperatures being related to relative sizes of the substituents and thus the unit cell volumes; modifications of the temperatures are sought here through combination of the two trivalent elements such as *Al* and *B* with different atomic sizes. *Al*/*B* containing alloys are known as good glass formers and the rapid solidification technique permits formation of a range of metastable phase in the system with improved solubility of the additives. Rapid solidification has been employed as a novel processing technique for the *Ni-Mn-Ga* alloys[11]. Limited substitutions were planned for *Ga* with *Al* to understand the role of the *Al* on transformation temperatures. Alloy composition $Ni_{50}Mn_{30}Ga_{15}Al_{5-x}B_x$ (x = 1 and 4) have been prepared, processed through melting and heat-treatment route. The results obtained are compared with the results reported earlier for $Ni_{50}Mn_{30}Ga_{15}Al_5$ alloy[7]. The alloys $Ni_{50}Mn_{30}Ga_{15}Al_{5-x}B_x$ (x = 0, 1, and 4) have also been processed through rapid solidification route to compare the effect of processing in addition to the compositions. The results of these studies are presented in this paper.

2. EXPERIMENT

50 g of each alloy has been prepared using high purity elements (<3N purity) in argon atmosphere by repeated arc melting to ensure homogenization. Alloy compositions $Ni_{50}Mn_{30}Ga_{15}Al_{5-x}B_x$ (x = 0, 1, and 4) were prepared and are designated as 'A', 'B' and 'C' respectively. The alloy 'A' has been reported as cast and heat-treated 1273 K for 3 h in a vacuum furnace and gas quenched[7]. The alloys 'B' and 'C' in the present study were cast and heat-treated in sealed evacuated quartz ampoules in a vacuum furnace at 1273 K for 72 h for homogenization followed by treatment at 1073 K for 48 h for improved ordering and then water quenched. The compositions of the alloys were determined from different places of the

Received 23 November 2011, revised 04 June 2012, online published 06 July 2012

ingots using inductively coupled plasma-optical emission spectroscopy (ICP-OES), energy dispersive x-ray spectroscopy (EDS) and electron probe micro analysis (EPMA) techniques. About 20 g of the heat-treated alloys were rapidly solidified using a melt spinner. The alloys were put into the crucible for the melt spinning; melt spinner evacuated to high vacuum and back filled with high purity argon to 600 mm pressure. After induction melting, the melt was ejected onto a rotating copper wheel (wheel speed 32 m/s).

Micro-structural examination of the heat-treated samples was carried out on a Leo 440 scanning electron microscope. Melt spun ribbons were examined on FEI Tecnai G2 transmission electron microscope using 200 kV. Thin foils of 3 mm dia for this purpose were milled on a GATAN-precision ion polishing system (PIPS) holder using initially at 5 kV and subsequently at 4 kV in varying angles of the ion gun. Room temperature X-ray diffraction patterns were taken on a Philips PW1320 diffractometer with CuK_{α} radiations. The transformation temperatures have been measured using differential scanning calorimeter (DSC) model Q100 (make TA instruments) under a constant heating/cooling rates of 20 K/min. Vibrating sample magnetometer (ADE make EV-9) was used for thermo-magnetic measurements and magnetic measurements up to 20 kOe at room temperature. Thermo-magnetic measurements were carried out at different temperatures with low bias magnetic field of 500 Oe. The discreet changes in magnetisation have been related to the structural and magnetic transitions.

3. RESULTS

The nominal and analysed compositions of the heat-treated alloys are shown in Table 1. The BSE images for the heat-treated alloy 'B' and 'C' alloys are shown in Fig 1. In addition to the matrix phase, these alloys showed presence of secondary phases. Different phase contrasts of a darker and a grayish phase distributed in the matrix could be seen. However, it is not clear whether the darker phase has resulted from ploughing out of the grayish phase during polishing. Considering the nature of contrast in BSE images as the atomic number contrast, the low atomic number elements *viz. Al/B* in the alloys may have gone to the secondary phases. Both the boron containing alloys 'B' and 'C' are multi-phase alloys unlike the boron free alloy 'A' in previous report.

The x-ray diffraction patterns obtained from the heat treated alloys 'A','B' and 'C' are shown in Fig. 2(a). While microstructure of the alloys 'B' and 'C' showed secondary phases (Fig. 1), the diffraction pattern for these alloys could be indexed to a non-modulated tetragonal martensite structure. No un-indexed peaks could be observed possibly due to overlap of the strong peaks of the secondary phase with those of the indexed matrix phase. The peak broadening increases considerably for the higher boron alloy. The marked peak positions show the structure to be the similar to that with low boron alloy 'B' with a very small shift to higher angle side with increasing boron. Figure 2(b) shows the x-ray diffraction patterns of the melt spun ribbons. All the obtained reflections

Table 1. Nominal and analysed compositions of the heat-treated alloys

Alloy design-ation	Nominal composition					Analysed composition									
	Atom %					Wt %					Equivalent atom %				
	Ni	*Mn*	*Ga*	*Al*	*B*	*Ni*	*Mn*	*Ga*	*Al*	*B*	*Ni*	*Mn*	*Ga*	*Al*	*B*
A	50	30	15	5	0	49.91 ±0.19	29.80 ±0.16	17.65 ±0.22	2.64 ±0.09	-	48.76	31.11	14.52	5.61	0
B	50	30	15	4	1	50.14 ±0.29	29.54 ±0.43	18.83 ±0.26	1.44 ±0.03	0.145 ±0.001	49.41	31.11	15.62	3.09	0.77
C	50	30	15	1	4	51.21 ±0.71	29.79 ±0.26	19.61 ±0.16	0.11 ±0.002	0.361 ±0.01	50.33	31.29	16.22	0.24	1.92

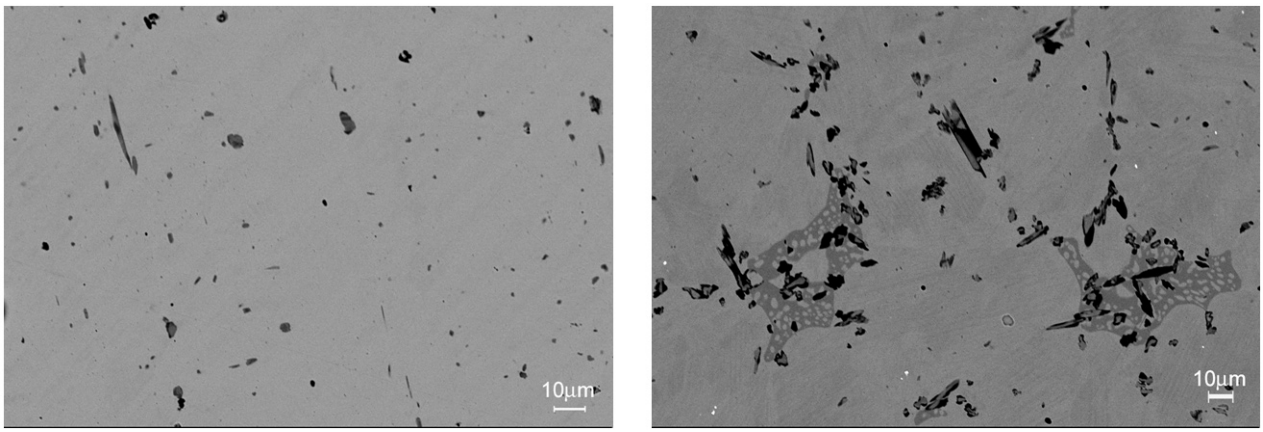

(a) **(b)**

Figure 1. The BSE images for the heat-treated alloys (a) alloy 'B' and (b) alloy 'C'.

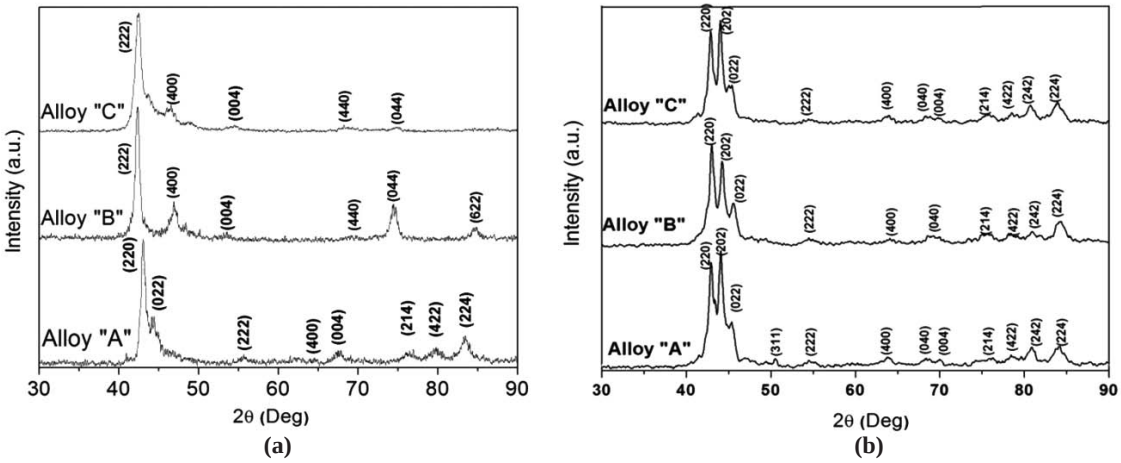

Figure 2. The X-ray diffractograms of (a) heat-treated alloys 'A', 'B' and 'C' and (b) melt spun alloys 'A', 'B' and 'C'.

indicate a 7-M martensite phase. The obtained patterns differ only in the relative intensities of the peaks but reflection positions are almost identical. Thus, the lattice parameters do not change significantly. Figure 3(a) shows the TEM bright field image of the ribbon of alloy 'A'. The image shows twinned martensite structure as well as areas free from twins, indicating the presence of untwinned martensite or a different phase. The selected area diffraction (SAD) pattern taken from untwinned portion (marked with a circle in Fig. 3(a)) is shown in Fig. 3(b). The diffused ring pattern obtained reveals the presence of an amorphous structure in the alloy. Figure 3(c) shows the SAD pattern from the martensite area and is indexed with zone axis $[\bar{1}11]$. The noticeable features of the SAD pattern are streaking of the major spots in certain direction as well as satellite spots. The spots in <101> direction do not show any streaking and thus, <101> is the common direction between the twins or the twin plane. The streaking in spots of (202) and (022) could be related to the twinned structure and conformed to the orientation relationship seen for the twin orientation in Fig. 3 (a). The satellite spots could be indexed to super-lattice spots from modulated 7 M martensite also referred as 14 M in orthorhombic coordinates similar to those reported earlier in *Ni-Mn-Ga* alloys[12]. The SAD pattern obtained, is thus consistent with the x-ray diffraction pattern obtained for this alloy ribbons (Fig. 2(b)). The ribbons of alloys 'B' and 'C' showed the similar matrix phase structure but with different microstructural features. The primary martensite plates in ribbons of alloy 'B' showed more than two variants of the martensite in some areas. Ribbons of alloy 'C' showed signs of fall of non-adherent particles suggesting two phase structure of the alloy ribbons (Fig. 4(a)). The matrix phase morphology noticed for this composition was faceted crystals (Fig. 4(b)) instead of spherical morphology for the alloy 'A' and 'B'.

The DSC thermograms of the heat-treated alloys and melt spun ribbons are presented in Fig. 5. The transformation temperatures observed from the thermograms are compiled in Table 2. The values for the heat-treated alloy 'A' in Fig. 5(a) have been included from the previous report for comparison. Only one transformation was noticed for the heat-treated alloys 'B' and 'C' in contrast to the alloy 'A' with two stage transformation. The transformation temperatures have increased with the increased boron in the alloys. The alloy 'C' with high boron showed a large thermal hysteresis of ~90K. Only a single transition is observed for all the compositions in melt spun state (Fig. 5(b)). A sharp transformation peak was obtained for the alloy 'A', whereas the alloys 'B' and 'C'

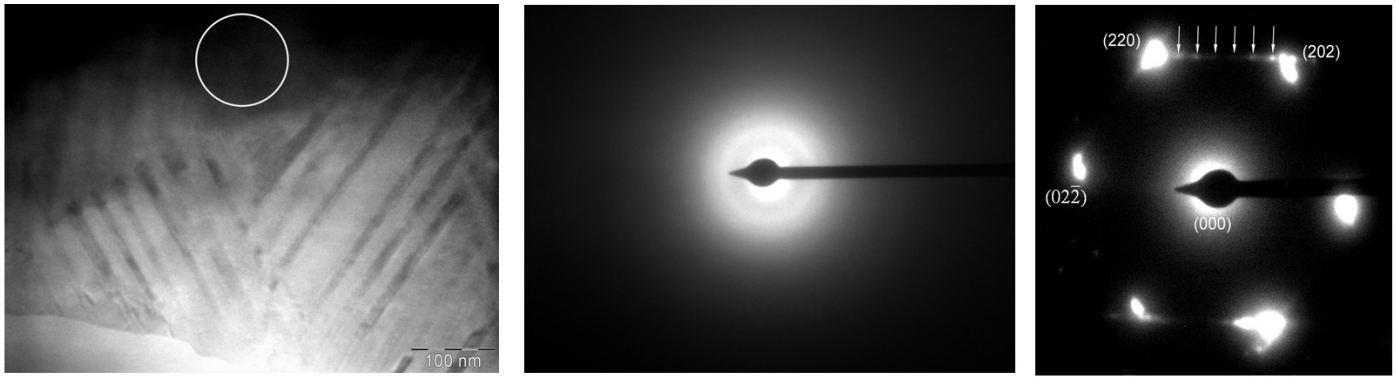

Figure 3. (a) The TEM picture of alloy 'A' showing martensite plates along with other phase and (b) SAD pattern from the area circled in (a) showing the diffused ring pattern of amorphous phase, (c) SAD pattern from martensite plates showing the 7 M martensite phase.

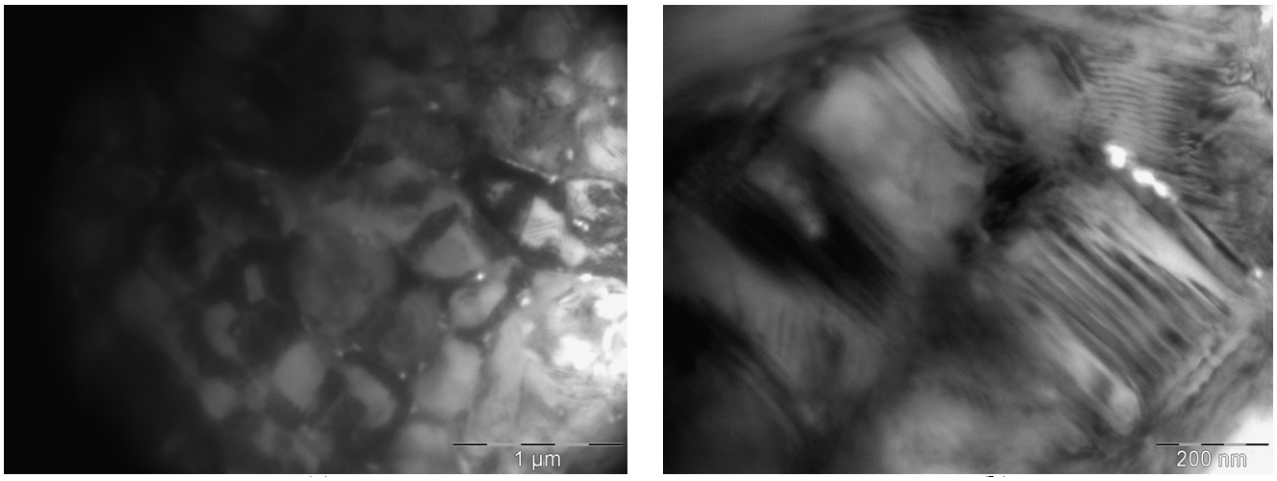

(a) **(b)**

Figure 4. (a) TEM image of alloy 'C' showing cellular structure with bright spots indicative of fall of non-adherent particles, and (b) enlarged cells from some area from (a) showing plates within the cell.

Table 2. Transformation temperatures through DSC for the alloys

Alloy	Stage	Cast and heat-treated alloys					Melt spun alloy ribbons				
		Martensite transformation temp (K)		Austenite transformation temp (K)		Thermodynamic equilibrium temp (K)	Martensite transformation temp (K)		Austenite transformation temp (K)		Thermodynamic equilibrium temp (K)
		Start (T_{Ms})	Finish (T_{Mf})	Start (T_{As})	Finish (T_{Af})		Start (T_{Ms})	Finish (T_{Mf})	Start (T_{As})	Finish (T_{Af})	
A	1	335	*	272	304**	342.5#	367	346	357	378	362.5
	2	*	302	304 $	350						
B	1	390	361	368	393	391.5	373	348	352	383	378
C	1	527	440	450	540	533.5	368	344	356	377	362.5

* Unresolved overlapping transition; ** end of intermediate stage 1;
$ start of intermediate stage 2; # Value for austenite to first martensite phase

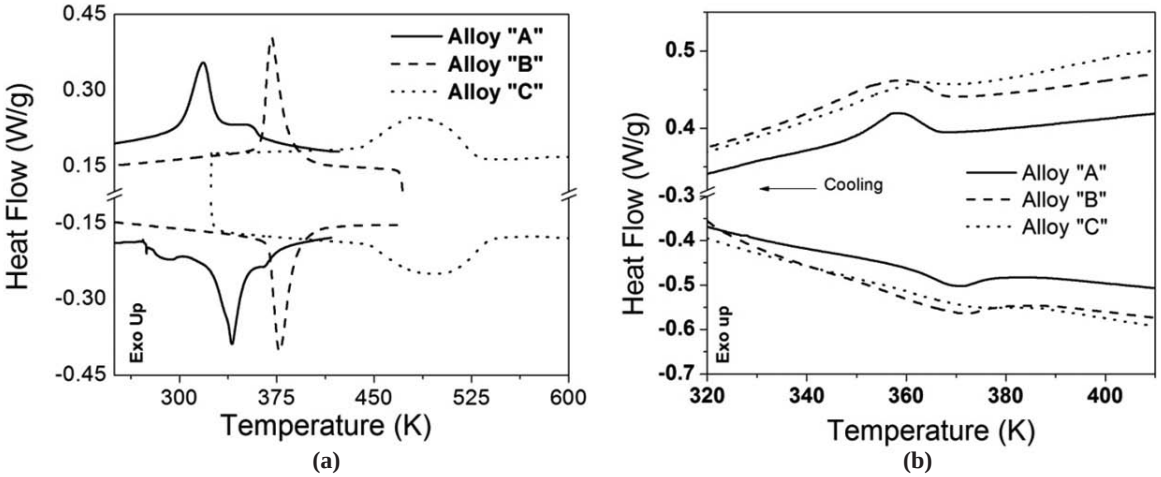

(a) **(b)**

Figure 5. The DSC thermograms for (a) heat-treated alloys and (b) melt spun alloys.

showed diffuse transitions. The highly diffuse transition for the alloy 'B' did not allow clear demarcation of the peak start/finish and the values in the Table 2, determined by the tangent intersection method, are indicative only. Due to the shape of the diffuse peak, the peak area indicative of the transformation enthalpy could not be compared here.

Figure 6 shows the thermo-magnetic M-T plots for the alloys. Plot of heat-treated alloy 'A' from previous report[7] under a biasing field of 500 Oe has been added in Fig. 6(a) for comparison. The heat-treated alloy 'A' revealed three transitions a rise beyond 302 K with a change of slope at 326 K indicated by arrow 1 in Fig. 4 prior to transition to paramagnetic state.

The alloys containing boron also showed change of slope with increasing temperatures; however the rate of change of slope does not show a rise but a different rate of fall. The point of rate of change marked with arrow 2 in the figure is in conformity with T_{Ms} temperature noted through DSC measurements whereas the lowering due to Curie transition is indicated by arrow 3. The phase specific set of magnetic properties viz. saturation magnetization and anisotropic field may cause either an increase or a decrease in magnetization with temperature rise and both deviations are signatures of the underlying transformation. The Curie temperatures noted through these measurements are 357 K for the alloy 'A' and 570 K for the alloys 'B' and 'C'. Plots for melt spun ribbons (Fig. 6(b)) show a continuous fall in magnetization with increasing temperature. However, the magnetization did not fall to zero within the measurement range. A linear fall excepting an intermediate rise in the temperature range from 300 K to 350 K, is noticed for the all the alloy ribbons. While the rise in magnetization with temperature may be attributed to martensite transformation in analogy with other alloys in the present study, the fall patterns do not match with the clear Curie transition noticed for the other alloys. This behavior, however, appears to be due to phase mixtures with different Curie temperatures. The melt spun alloy 'A' clearly shows a rapid fall after the martensite transition and then a slower fall showing the manifestation of two phase Curie temperatures. It may be noted here that like the DSC measurements, the sharpness of transition decreased in the sequence 'A' to 'C' and then 'B'. The transition temperature range noticed through these measurements is also similar to those obtained from DSC measurements.

The room temperature magnetization curves of the alloys are shown in Fig. 7. The magnetization observed are of 47.0 emu/g, 6.5 emu/g, and 8.8 emu/g for the heat-treated alloys 'A','B' and 'C' respectively with an applied field of 12 kOe. It may be noted that the M-H curve has not reached saturation for the alloys 'B' and 'C'. While the curves retraced themselves for these alloys on removal of the magnetic field, alloy 'A' showed a hysteresis with coercivity value of 370 Oe. The alloy ribbons of 'A', 'B' and 'C' showed magnetization values of 13.0 emu/g, 7.8 emu/g and 6.3 emu/g at 20 kOe. The inset in the Fig. 7(b) shows a blow-up of the plot around the origin All the alloys showed hysteresis during reverse magnetization and the coercivity values obtained (Fig. 5(b) inset) were 183 Oe for alloy 'A' and 280 Oe for the boron containing alloys 'B' and 'C'.

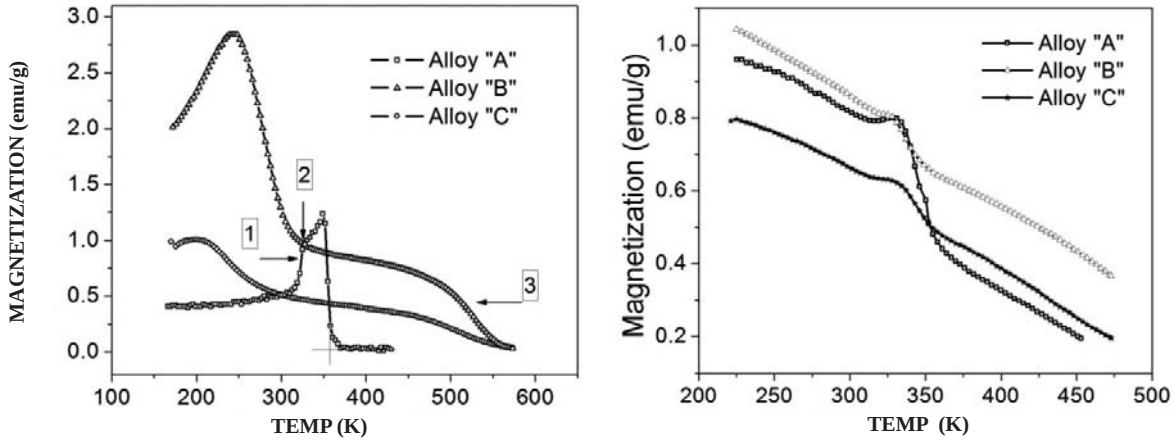

(a) (b)

Figure 6. The thermo-magnetic M-T plots for (a) heat-treated alloys and (b) melt spun alloys.

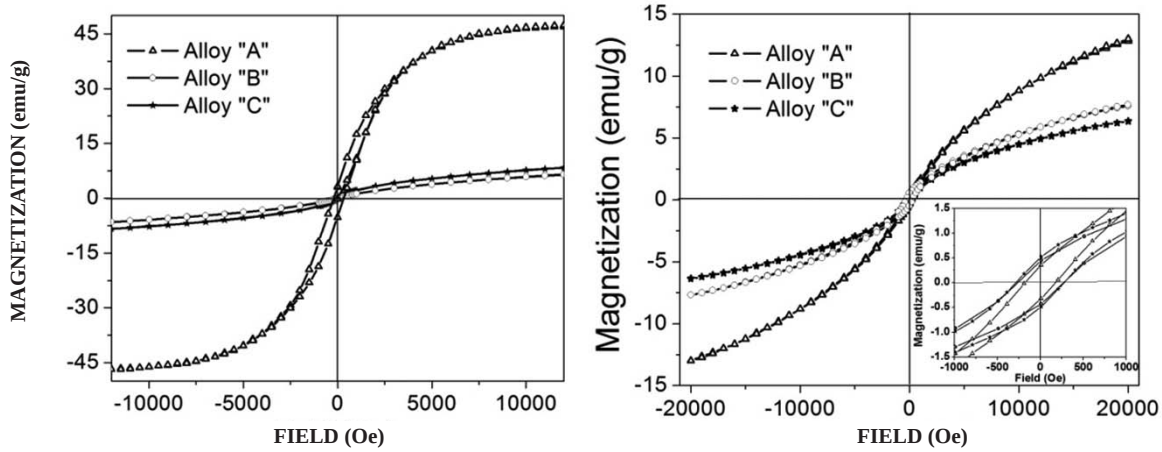

(a) (b)

Figure 7. Room Temperature magnetization curves for (a) heat-treated alloys and (b) melt spun alloys. Inset in (b) shows an enlarged view around origin.

4. DISCUSSION

The alloys with trivalent elements *Al/B* replacing *Ga* have shown different microstructures and crystal structures at different compositions and different processing conditions. While the alloy with 5 at% Al has been reported to be a single phase structure, boron containing alloy ribbons shows multi-phase structures. The quantities of second phase are generally within detectable limits of x-ray diffraction, however, many of the diffraction peaks from the second phase might have similar inter-planar spacing as the matrix phase. Limited number of distinct peaks for the phase did not permit structure identification of this phase observed in the alloys containing boron. In view of the presence of low atomic number element boron, present in these samples, a meaningful EPMA analysis is not possible. Darker contrast of the secondary phase than the matrix in BSE images of the alloys indicates enrichment of this phase by elements of higher atomic number. This observation also signifies relatively higher presence of low atomic number elements like B and Al in the matrix phase. It may be noted that the crystal structure of the alloy 'A' is that of modulated martensite which changes to a non modulated structure with addition of B in the alloy. Even though small size difference exists between the constituents of ternary *Ni-Mn-Ga* alloys, these elements are in close vicinity of each other in the periodic table. The similarities permitting modulated long period arrangements are compromised by the addition of boron and hence the change to non-modulated structure. Table 3 summarises the crystal structure data obtained through x ray diffraction measurements for the matrix phase in our alloys.

The rapid solidification process has been employed for obtaining metastable phase structures in these alloys. The process normally does not permit separation of the phases because of faster cooling and the x-ray diffractograms of melt spun ribbons could be indexed fully to a 7M martensite phase similar to those reported for the ternary *Ni-Mn-Ga* alloys without any un-indexed peaks to suggest absence of any secondary phase. The x-ray peak positions obtained for the different alloys are very close to permit any distinction in terms of the lattice parameters. The lattice parameters are normally a function of compositions and/ or lattice strains. With similar processing treatment, the x-ray diffractograms without any perceptible variation in the peak position are indicative of similar composition of the phase indexed by x-ray diffraction pattern. The TEM microstructures of the rapidly solidified ribbons show the presence of additional phases such as amorphous phases in case of alloy 'A' ribbons; or non-adherent chemically different phases falling out of the thinned TEM specimens in case of 'C' ribbons. Boron is reported to promote glass formation in Fe based alloys with glassy phase crystallizing into the boride phases on heating[13]. Such metastable phases may have appeared due to sluggish crystallization in rapidly solidified ribbons. The amount of amorphous phase is expected to increase with addition of boron. But, no amorphous phase could be located in different specimens of alloy 'B' ribbon samples. The alloy ribbon 'C' indicate presence of non-adherent phase in TEM micrograph. With the chemical composition of the matrix phase showing little or no variation through diffractograms of the alloys 'A','B' and 'C', it is reasonable to assume that the second phase in these ribbons could have been a boron rich phase. The rapid quenching at still higher cooling rates to suppress phase separation is, however, not attempted as the aim has been to obtain metastable crystalline phases and not amorphous phases.

Though the crystalline matrix phase present in our melt-spun ribbons shows similar structure as well as the same unit cell size, the morphology of the pre-martensite is found to be different. Alloys 'A' and 'B' show spheroidal grains but faceted grains are observed in case of alloy 'C' ribbons. Faceted crystal formation shows that the interfacial energies at different faces of the crystals are different, which may have facilitated formation of polyhedral grain boundary in boron rich alloy. With isotropic nature of the amorphous phase, the spherical grain shape is expected as it has been observed in 'A' and 'B' alloy ribbons. The faceted grains show a change in interfacial energies because of the presence of boron, which may segregate to grain boundary and result in non-adherent boron rich phase coming out from the grain boundary area.

The unit cell volume of 191.92 Å^3 for the 5M martensite structure in the alloy 'A' compares well with the value of 197.2 Å^3 obtained for a ternary $Ni_{50.1}Mn_{29.1}Ga_{20.8}$ alloy with 5M structure[14]. Modifications in properties on addition of trivalent Al in place of *Ga* are expected only through modification of inter-atomic distance without any change in average electron to atom ratio. The boron additions have been attempted to modify inter-atomic distances significantly without changing average electron to atom ratios. Heat-treated alloys containing boron, however, have shown non modulated structure observed in ternary *Ni-Mn-Ga* alloys. The c/a ratio of the alloys fell with increasing boron from 1 at% to 4 at%. Unit cell volume is expected to decrease with increasing boron and decreasing Al; however, a small rise in cell volume is noticed in going from alloy 'B' to 'C'. With BSE images suggesting boron to be present within the matrix phase, it is possible that boron may have gone to interstitial sites instead of substituting at the

Table 3. Martensite phase and lattice parameters for the heat-treated and rapidly solidified alloys

Alloy	Heat-treated alloys					Rapidly solidified ribbons						
	Structure[#]	Lattice parameters		c/a	Cell vol. (Å^3)	Structure[#]	Lattice parameters			c/ a	b/a	Cell vol. (Å^3)
		a (Å)	c (Å)				a (Å)	b (Å)	c (Å)			
A	5M	5.87	5.57	0.95	191.92	7M	6.05	5.67	5.54	0.91	0.93	190.04
B	NM	7.67	6.83	0.89	401.80	7M	6.05	5.67	5.54	0.91	0.93	190.04
C	NM	7.78	6.69	0.86	404.93	7M	6.05	5.67	5.54	0.91	0.93	190.04

[#] NM indicates Non-modulated tetragonal and 5M & 7M indicate modulated martensite structures.

Ga site as envisaged. Thus, boron addition may result in only small cell volume change in alloys containing boron.

Ternary $Ni_{47.3}Mn_{33.1}Ga_{18.6}$ alloy containing lower *Ga* are reported to possess a 14M orthorhombic cell with lattice parameters of a = 5.8466, b = 6.1432 and c = 5.5391Å and a lattice volume of 198.49 Å^3. Lattice parameters obtained for our 7 M martensite phase in ribbons are comparable to these values albeit a smaller lattice volume. It may be noted that parameters for the 7 M phase obtained is the same for different alloys, and the composition changes may have been accommodated in the secondary phase below detection limits of x-ray diffraction but observed in TEM images. The lower lattice volumes in ribbons may be attributed to lower atomic ordering associated with the rapid solidification technique.

The heat-treated alloy 'A' showed a two-stage martensite transformation. Martensite transformations are reported to go through a sequence of the intermediate martensite phase[15]. Low temperature diffraction patterns are not available to decide the transformation sequence unambiguously. The temperature $T_0 = (T_{Ms}+T_{Af})/2$ is normally taken as the thermodynamic equilibrium temperature between the martensite and austenite phase and is considered dependent on the chemistry whereas the transformation temperature ranges depicting the nucleation of the phases may be structure dependent[16]. Addition of *B* for *Al* results in increasing the martensite transformation temperature almost linearly whereas T_c increases to saturate at higher boron. The martensite transformation normally occurs when the Fermi surface reaches the Brillouin zone boundary with increasing number of valence electron and the alteration in the Brillouin zone boundary may affect the martensite transformation temperature[17]. The packed structures normally increase the transformation temperatures. The lattice volume of the alloys 'B' and 'C' containing boron is comparable however with different c/a ratios. The c/a ratio of the 4% *B* alloy is 0.86 compared to 0.89 for the alloy with 1% *B*. Though the exact density of states calculation is not available for these alloys, it appears that the compact structure along c-axis has resulted in increase of the martensite transformation temperature. The T_0 temperatures for the melt spun ribbons do not change with compositions and this observation is consistent with the similar crystal structure parameters of the alloy ribbons.

The martensite transformation temperature range for the high boron alloy is ~ 90K. The reversibility of the martensite transformation is related to the thermal hysteresis between the martensite transformation and reverse martensite to austenite transformations. Transformations occurring with large thermal hysteresis are not reversible and are accordingly referred as thermoplastic transformations in contrast to thermo-elastic or reversible transformation with smaller thermal hysteresis[15]. The large thermal hysteresis i.e. thermo-plasticity indicate that re-nucleation of the austenite phase in the transformed martensite is difficult. Alloys with thermoplastic martensite transformation or with non-modulated martensite do not show reversible transformation and may not be suitable for technological applications.

The saturation magnetization of the alloy 'B' is 6.5 and 7.8 emu/g in the heat treated and melt spun conditions. The alloys 'A' and 'C' show decrease in saturation magnetization values with rapid solidification processing. Both the processing methods show lowered magnetization with increasing boron content. Even though the crystal structure obtained is different in the two processing techniques, existence of similar structures obtained as for other ternary *Ni-Mn-Ga* alloys indicates that the inter-atomic distances between the constituent elements have not changed considerably. The saturation magnetization is affected by the exchange interaction between the atomic magnetic moments and this interaction depends on the atomic distance between the constituent atoms as illustrated by classical Bethe –Slater curves. Change in magnetization in these alloys have been related to moments at Ni site varying with martensite structure[18,19]. A large fall in magnetization for the melt spun ribbon where neither the composition nor the average inter-atomic distances have changed considerably could be attributed to disordered structure resulting on rapid quenching. For the higher boron alloys, the addition of boron may cause loss of ordering even in heat-treated alloys and its overwhelming effect makes the influence of processing technique immaterial.

5. CONCLUSIONS

Addition of *Al* or *Al* and *B* with intention to replace trivalent *Ga* in a ternary base composition of $Ni_{50}Mn_{30}Ga_{20}$ has been studied. With average e/a ratio unchanged, the properties of the alloys get considerably modified due to change in inter-atomic spacing. Addition of B along with Al results in formation of a two-phase structure and martensite structure changed to non–modulated tetragonal martensite in place of 5 M modulated martensite obtained with *Al* addition alone, possibly because of the small sized boron atoms destroying modulation by its ability to occupy interstitial sites randomly. The rapid solidification processing of the alloys results in a modulated 7 *M* martensite structure for the three compositions investigated with variations in composition accommodated in secondary phases.

The range of temperature over which martensite transformation occurs, is much higher for alloy 'C' with highest *B* content for the heat-treated alloys. A wider martensite transformation temperature range of ~90 K for high *B* alloy shows that in spite of improved martensite stability, the reversibility of transformation is adversely affected by *B* addition. No significant changes in martensite transformation temperatures were noticed commensurate with unchanged chemistry of the 7M martensite phase. The saturation magnetization decreases with *B* addition significantly for both heat-treated and the rapidly solidified conditions. The magnitude of decrease is much larger than the dilution effects showing lowered magnetic exchange between the transition elements.

ACKNOWLEDGEMENTS

The authors are thankful to Defence Research & Development Organization (DRDO), India for the financial support through a project. Authors express their thanks to Dr G. Malakondaiah, Director, Defence Metallurgical Research Laboratory, Hyderabad for his constant encouragement and permission to publish these results.

REFERENCES

1. Wilson, S.A.; Jourdain, R.P.J.; Zhang, Q.; Dorey, R.A.;Bowen, C.R.;, Willander, M. & Wahab, Q.U. New Materials for micro-scale sensors and actuators: An engineering review. *Mater. Sci. Engg.*, 2007, **56**(1-6), 1-129.
2. Ullako Huang, K.J.; Kantner, C.; Handley, R.C.O. & Kokorin, V.V. Large magnetic field induced strains in *Ni*2*MnGa* single crystals. *Appl. Phys. Lett.*,1996, **69**(13),1966-68
3. Kakeshita, T. & Ullakko, K. Giant magnetostriction in ferromagnetic shape-memory alloys. *MRS Bulletin*, 2002, **27**(2), 105-09.
4. Soderberg, O.; Sozinov, Y.Ge.A.; Hannula, S.P. & Lindros, V.K. Recent breakthrough development of the magnetic shape memory effect in *Ni–Mn–Ga* alloys. *Smart Mater. Struct.*, 2005, **14**(5), 223-235.
5. Wuttig, M.; Liu, L.; Tsichiya, K. & James, R.D. Occurrence of ferromagnetic shape memory alloys. *J. Appl. Phys.*, 2000, **87**(9), 4707-11.
6. Chernenko, V.A. Compositional instability of β-phase in Ni-Mn-Ga alloys. *Scripta Materialia.*, 1999, **40**(8), 523-27.
7. Mathur, R.P.; Singh, R.K.; Chandrasekaran, V.; Ray, S. & Ghosal, P. Structural and magnetic transitions in *Fe*-, *Co*- and *Al*-substituted *Ni-Mn-Ga* ferromagnetic shape memory alloys. *Metal. Mater. Trans. A*, 2007, **38**(9), 2076-84.
8. Entel, P.; Bucholnikov, V.D.; Khovailo, V.V.; Zayak, A.T.; Adeagbo, W.A.; Gruner, M.E.; Harper, H.C. & Wasserman, E.F. Modelling the phase diagram of magnetic shape memory Heusler alloys. *J. Phys. D: Appl. Phys.*, 2006, **39**(5), 865
9. Jin, X.; Marioni, M.; Bono, D.; Allen, S.M. & O'Handley, R.C. Empirical mapping of *Ni-Mn-Ga* properties with composition and valence electron concentration. *J. Appl. Phys.*, 2002, **91**(10), 8222-24.
10. Singh, R.K.; Shamsuddin, M.; Gopalan, R.; Mathur, R.P. & Chandrasekaran, V. Magnetic and structural transformation in off-stoichiometric *NiMnGa* alloys. *Mater. Sci. Engg., A*, 2008, **476**(1-2), 195-200.
11. Panda, A.K.; Kumar, A.; Ghosh, M. & Mitra, A. Development of NiMnGa-based ferromagnetic shape memory alloy by rapid solidification route. *J. Magn. Magn. Mater.*, 2008, **320**(20), 730-33
12. Bennett, J.C.; Hyatt, C.V.; Gharghouri, M.A.; Ferrell, S.; Robertson, M.; Chen, J. & Prirge, G. In situ transmission electron microscopy studies of directionally solidified *Ni–Mn–Ga* ferromagnetic shape memory alloys. *Mater. Sci. Eng.* A , 2004, **378**(1-2), 409-14.
13. Mathur, R.P., Murthy, V.N.; Akhtar, D.; Subrahmanian, P. & Jagannathan, R. Crystallization processes in amorphous $Fe_{74}Co_{10}$–xCr_xB_{16} alloy. *J. Mater. Sci. Lett.* 1987, **6**, (9), 1019-22
14. Richard, M.; Feuchtwanger, F.; Schlagel, D.L.; Lograsso, Allen, S.M. & O'Handley, R.C. Crystal structure and transformation behavior of *Ni–Mn–Ga* martensites. *Scripta Mater.* 200, **54**(10), 1797-1801
15. Segui, C.; Pons, J. & Cesari, E. Effect of atomic ordering on the phase transformations in *Ni–Mn–Ga* shape memory alloys. *Acta Mater.*, 2007, **55**(5), 1649-55
16. Otsuka, K. & Wayman, C.M. Shape memory materials, Cambridge University Press 1998, UK.
17. Entel, P.; Gruner, M.E.; Adeagbo , W.A.; Eklund, C.J.; Zayak, A.T.; Akai, H. & Acet, M. Ab initio modeling of martensitic transformations (MT) in magnetic shape memory alloys. *J. Magn. Magn. Mater.*, 2007, **310**(2), 2761-63.
18. Singh, R.K.; Mathur, R.P.; Manivel, Raja, M. & Shamsuddin, M. Effect of *Fe* substitutions on the phase stability and magnetic properties of Mn-rich *Ni-Mn-Ga* ferromagnetic shape memory alloys. *J. Magn. Magn. Mater.*, 2011, **323**(5), 574-578
19. Singh, R.K.; Manivel Raja M.; Mathur, R.P. & Shamsuddin, M. Magnetic structure of modulated martensite phase in Ferromagnetic Shape Memory NiMnGa alloys. *Mater. Chem. Phys.*, (In press)

Contributors

Dr R.P. Mathur obtained BE from Rajasthan University, Jaipur, and MTech from Indian Institute of Technology, Kanpur, in 1982 and 1991, respectively. He has obtained his PhD from Indian Institute of Technology, Roorkee, in 2008. Presently, he is working as a Scientist at Defence Metallurgical Research Laboratory (DMRL), Hyderabad. His areas of research interest include: amorphous alloys, nanostructured soft/hard magnetic materials, rare earth permanent magnets, functional materials such as shape memory alloys. He has published about 25 research papers in reputed international journals and more than 30 papers in national/ international conference proceedings.

Mr R.K. Singh obtained his BTech (Metallurgical Engineering) from the Indian Institute of Technology, Roorkee, and MTech (Metallurgy) from Institute of Technology, Banaras Hindu University, Varanasi, in 2002 and 2006, respectively. Presently, he is working as a Scientist at DMRL, Hyderabad. His research area includes: development of ferromagnetic shape memory alloys, *Ni-Ti* based shape memory alloys, *Sm-Co*-based permanent magnets and other magnetic materials for defence applications.

Prof (Dr) Subrata Ray obtained his MTech and PhD from IIT, Kanpur. Presently, he is working as Professor, Metallurgical and Materials Engineeringin University of Roorkee. He has research interests in materials development with special emphasis on cast metal matrix composites (MMC). He has many pioneering contribution in cast MMC including introduction of stir-casting and addition of surface active elements for which he held the first patent. He has also developed interest on materials used in Li-ion batteries. He has published more

than 200 technical papers, mostly in international journals and handbooks including those of ASM and ASLE. He is a fellow of the National Academy of Sciences, India, and Indian National Academy of Engineering.

Dr Partha Ghosal obtained PhD in Metallurgical Engineering from IT, Banaras Hindu University in 1996. Presently, he is working as a Scientist in the Electron Micoscopy Group at DMRL. He is recipient of Young Microscopists Award (2001) from EMSI and DRDO–Laboratory Scientist of the Year Award (2006). His research interests are nanomaterials cha-racterisation and defects characterisation using electron microscopy and has more than 15 years of experience. He has published 35 research papers in reputed international journals and more than 45 papers in national/international conference proceedings/presentations. He has delivered 25 invited lectures and is the author of 2 patents. He is a life member of IIM, EMSI, MSI and MRSI.

Dr V. Chandrasekaran obtained his PhD from Annamali University, Tamil Nadu. He is Ex-senior scientist of DMRL. His areas of research interest include: Rare earth permanent mag-nets, magnetostrictive, magnetocaloric, ferromagnetic shape memory and nanostructured soft/hard materials. He has published more than 40 papers in international journals. He was a recipient of MRSI medal (1990), Vasvik Industrial Research Award (1991) and Metallurgist of the Year Award (1998).